Design and Analysis of a Self-Excited Brushless Wound-Field Synchronous Machine with Reduced Torque Ripple

HAQ, Muhammad Ashan ul, FAROOQ, Haroon and AKMAL, Muhammad <http://orcid.org/0000-0002-3498-4146>

Citation:

HAQ, Muhammad Ashan ul, FAROOQ, Haroon and AKMAL, Muhammad (2026). Design and Analysis of a Self-Excited Brushless Wound-Field Synchronous Machine with Reduced Torque Ripple. International Transactions on Electrical Energy Systems, 2026 (1): 3692957. [Article]

International Transactions on Electrical Energy Systems

WILEY

RESEARCH ARTICLE OPEN ACCESS

Design and Analysis of a Self-Excited Brushless Wound-Field Synchronous Machine With Reduced Torque Ripple

Muhammad Ahsan ul Haq[1] | Haroon Farooq[2] | Muhammad Akmal[3]

[1]Department of Electrical, Electronics & Telecommunication Engineering, University of Engineering and Technology, Lahore (Faisalabad Campus), Faisalabad 38000, Punjab, Pakistan | [2]Department of Electrical Engineering (RCET), University of Engineering and Technology, Lahore 39161, Pakistan | [3]School of Engineering and Built Environment, Sheffield Hallam University, Sheffield S1 1WB, UK

Correspondence: Haroon Farooq (haroon.farooq@uet.edu.pk) | Muhammad Akmal (m.akmal@shu.ac.uk)

Received: 24 February 2026 | **Revised:** 29 June 2026 | **Accepted:** 8 July 2026

Academic Editor: Changsong Cai

Keywords: brushless working | finite element analysis using JMAG | subharmonic component (0.5 order for brushless operation) | wound-field synchronous machine

ABSTRACT

Permanent magnet synchronous machines are commonly employed in variable-speed applications because they offer high efficiency, easy control, robust construction, and do not require external field excitation. However, rising costs of permanent magnets have significantly increased the overall price of these machines. Wound-field synchronous machines (WFSMs), which have no permanent magnets and are thus less affected by market price changes, can be a good alternative to permanent magnet synchronous machines. WFSMs use slip rings along with brush assemblies to energize the rotor field winding (RFW) with DC. However, the use of slip rings and brushes introduces sparking and increases maintenance requirements. Consequently, brushless wound-field synchronous machines (BLWFSMs) have recently been developed to overcome these limitations. This paper introduces a novel BLWFSM designed to mitigate the volatility of permanent magnet prices and the maintenance challenges of conventional WFSMs using slip rings and brushes. Unlike existing brushless topologies that necessitate dual inverters, the proposed design utilizes a single three-phase inverter. The proposed machine's rotor incorporates an excitation winding and a field winding, connected via an embedded rotating bridge rectifier. The stator MMF is dominated by a 30-Hz subharmonic component and a 60-Hz fundamental component. Brushless excitation is achieved by utilizing a subharmonic stator MMF component (30 Hz) that induces an AC voltage in the excitation winding, which is rectified by a rotating rectifier and supplied as DC to the field winding. Two-dimensional finite element analysis validates the performance of an 8-pole, 18-slot configuration. The results demonstrate a rated torque of 8.975 Nm with an exceptionally low torque ripple of 0.501%. These characteristics, combined with a reduced volume and weight profile, position the proposed BLWFSM as a robust alternative for air blowing, aerospace power generation, and electric vehicle applications.

1 | Introduction

For more than two centuries, electrical machines, including motors and generators, have played a pivotal role in technological advancement. Their applications span nearly every aspect of modern human life, ranging from household appliances, such as washing machines, fans, blenders, and vacuum cleaners, to industrial systems, including pumps, conveyor systems, and milling machines. As a result, electric motors are among the most essential electrical devices in the developed world [1–4]. Electrical generators, however, are responsible for supplying nearly all of the world's electrical energy through wind, hydro, and thermal power generation plants, thereby meeting both commercial and domestic energy demands [5–7]. In short, electrical motors and generators are the backbone of modern society.

Electrical machines have evolved into various types, including DC machines (brushed and brushless) and AC machines, such as synchronous, induction, reluctance, and vernier machines. Synchronous machines are further classified into two major types: (i) wound-field synchronous machines (WFSMs) and (ii) permanent magnet synchronous machines (PMSMs). Recent fluctuations in the cost of magnets employed in PMSMs have motivated researchers to explore alternative solutions, such as WFSMs and PM-assisted synchronous machines. In conventional wound-field synchronous machines (CWFSMs), rotor field excitation is provided through slip rings, brushes, and a separate excitation unit, which increases system size, cost, and maintenance due to continuous brush sparking. Some advantages of CWFSM compared to PMSMs are outlined as follows:

a. Low-cost rotor design as no permanent magnets (PMs) are required, and machine cost is independent of the price and availability of PMs.
b. Three independent control variables (i_d, i_q, i_f) provide additional optimization possibilities in CWFSM as compared to PMSMs, which only have i_d and i_q
c. Proper control of these three variables (i_d, i_q, i_f) can achieve a near-unity power factor.
d. The air-gap magnetic flux density is limited solely by the quality of the magnetic steel, originating high torque.

In comparison with PMSMs, the following are the disadvantages of CWRSMs:

a. Due to the continuous operation of the motor, the slip rings and brushes used in CWRSMs wear out, resulting in increased maintenance requirements.
b. There are additional copper losses in CWFSMs due to the excitation of the rotor field winding (RFW).
c. To excite the RFW of CWFSM with DC, a DC source is required, which results in an increase in the overall cost of the motor.

To overcome these limitations, several brushless wound-field synchronous machine (BLWFSM) topologies have been proposed [8–19]. In large machines, BL exciters supply DC to the generator, as shown in Figure 1. The BL exciter has field windings on the stator and the armature on the rotor, eliminating the requirement for carbon-based brushes and slip rings and minimizing maintenance. A pilot exciter is frequently incorporated to make the generator's excitation fully independent of external power. However, the exciter contributes to a larger and more costly system. Recent research has focused on brushless generators with integrated exciter winding configurations [20–24].

Ayub et al. [25] proposed an inverter scheme in which the current comprises both the fundamental component (FC) and an additional third harmonic component (3HC). BL operation of the WFSM is achieved by utilizing this 3HC. For BL operation, the machine requires two distinct windings, rotor harmonic winding (RHW) and RFW, which are linked through a rotating rectifier. However, the proposed machine requires a larger number of diodes due to pulse width modulation. Moreover, the machine exhibits significant torque ripple of 41.96% and 34.05% for the eighteen-slot, four-pole design and forty two-slot, four-pole configurations, respectively.

BL operation of WFSMs has been proposed in [26] by inducing a 3HC. The machine's armature winding (AW) was energized with currents by two different inverters operating at different frequencies. A regular 3-Φ FC with a frequency of 60 Hz is supplied by one inverter, while the neutral point of the AW of the proposed motor was connected to a second inverter, operating at

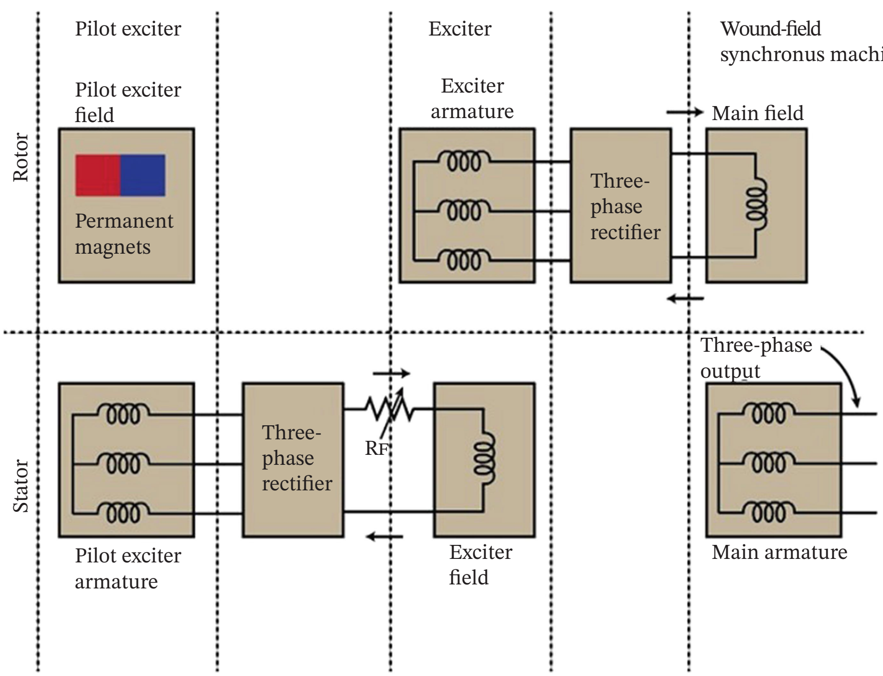

FIGURE 1 | BL excitation scheme including a pilot exciter.

180 Hz, which supplied a single-phase 3HC. The armature field is generated by FC, whereas 3HC induces voltages in RHW. After rectification, RFW is energized with DC without using brushes. The main limitation of the presented design is the requirement for two inverters, which results in a costly system.

Ref. [27] proposed a novel five-phase AW configuration to achieve BL operation of WFSMs. The five-phase AW generates both the fundamental and appropriately sized SH-MMF components. Among these two MMF components, the fundamental MMF produces the stator main field, while the SH-MMF develops AC in the RHW. A diode bridge rectifies this current to deliver DC excitation to the RFW without the use of brushes. However, the proposed machine exhibits significant torque ripple.

In Ref. [28], a novel BL self-excitation topology for WFSMs is presented. The proposed approach employs a multiphase AC stator (five phases or higher) to generate two independently controllable magnetic fields in rotating conditions with different spatial harmonic orders. Rotor windings are magnetically coupled by these two magnetic fields. The rotor incorporates RFW, transformer windings, and a rectifier. RFW is supplied by a DC voltage produced by the rectifier from the AC voltages of the rotor transformer windings. A five-phase stator is developed, and the machine's performance is analyzed using the finite element method. Simulation results at various operating speeds validate the performance for the proposed BL design. A comparative analysis of the torque and power characteristics was also performed between the proposed machine and comparable-sized interior PM and induction machines.

A new method to generate BL excitation for a WFSM using the creation and use of a subharmonic component of stator MMF (SH-SMMF) is discussed in [29], as shown in Figure 2. The technique uses a dual-inverter setup for the AW to produce both the fundamental MMF component and an extra SH-SMMF simultaneously. The rotor of the motor has two separate windings: REW and RFW. The SH-SMMF causes a voltage in REW. Subsequently, a single-phase rotating rectifier located on the rotor rectifies the output voltage of REW to provide DC to the RFW.

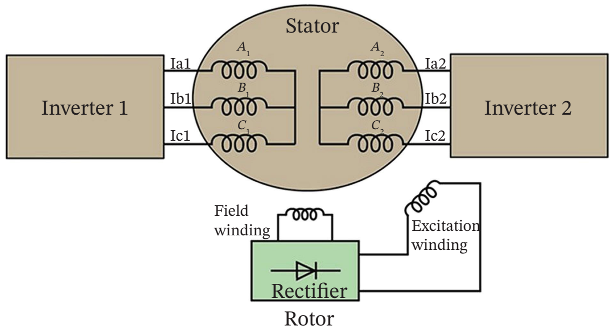

FIGURE 2 | Dual inverter–based BLWFSM topology.

The use of two inverters in the proposed design is the main concern of this setup, as it increases the total system cost.

Reference [30] discusses a BLWFSM topology that employs an uncontrolled 3-Φ rectifier installed on the stator side. The common point of the star-connected 3-Φ AW is connected to the rectifier output. A fundamental rotating MMF, along with a harmonic pulsating magnetic field, is generated by this configuration. The harmonic field generates harmonic currents in RHW. These harmonic currents are subsequently rectified to DC using a rectifier to excite the main RFW, thereby enabling BL operation. The fundamental rotating armature field magnetically couples with the field of the rotor to generate torque. The requirement of an uncontrolled rectifier at the stator side and a relatively high torque ripple magnitude of 51.30% are the two primary drawbacks of this topology.

The harmonic field excitation method for BL working of WFSMs is introduced in [31]. The scheme uses standard 3-Φ and 1-phase inverters working at different frequencies to inject current to AW simultaneously. Consequently, a combined inverter output creates a composite current with both fundamental and 3 HCs. The FC establishes the stator magnetic field, while the 3HC produces a pulsating MMF in the air gap. This pulsating MMF causes AC in the RHW, which is then rectified to get DC for the RFW. The use of two inverters and a significant torque ripple of about 66% are the main concerns of this topology.

TABLE 1 | Comparative assessment of the proposed brushless machine and brushless generator with embedded exciter.

Feature	Conventional brushless generator with embedded exciter	Proposed BLWFSM
Excitation method	Separate AC exciter with rotating rectifier	Subharmonic stator MMF–based self-excitation
System components	Main generator + exciter + (optional) pilot exciter	Single integrated machine
Power conversion stages	Multiple stages	Single-stage
Rotor configuration	Field winding fed via exciter and rectifier	REW + RFW with embedded rectifier
Brushes/slip rings	Not required	Not required
Size and weight	Larger and heavier	More compact and lightweight
Mechanical complexity	Higher	Lower
Control complexity	High	Lower
Efficiency	Lower (multiple stages)	Higher (reduced stages)
Cost	Higher (additional components and assembly)	Potentially lower (reduced component count)
Maintenance cost	Moderate	Lower
Applications	Large-scale generation	Compact systems (EVs, aerospace, and blowers)

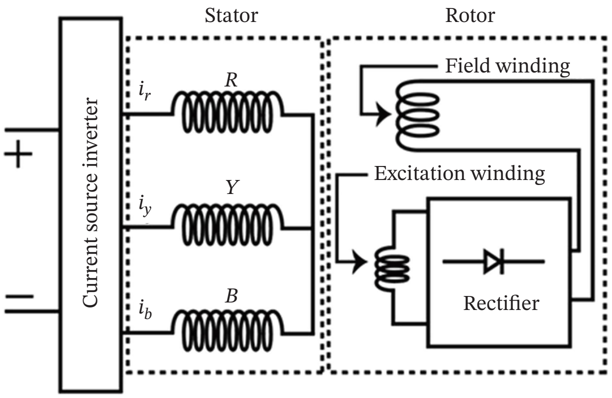

FIGURE 3 | Proposed WFSM brushless topology.

In [32], a novel BLWFSM topology is presented, incorporating a dual-frequency inverter system to produce a SH-SMMF. ABC and XYZ are the two windings present on the stator. Similarly, the rotor is comprised of two windings: RHW and RFW. The ABC winding, having an 8-pole configuration, works at the fundamental frequency, whereas the XYZ winding, having a 2-pole configuration, functions at twice the fundamental frequency. This coordinated operation produces a controlled SH-SMMF with a magnitude equal to one-fourth of the FC- SMMF. An EMF is induced in the RHW by the SH-SMMF. Induced AC from the SH-SMMF is captured by the RHW and converted to DC via a rectifier; this DC then excites the RFW, eliminating the need for brushes. The use of two inverters supplying different frequency signals to separate stator windings (SWs) and lower efficiency are the main concerns of this topology.

Reference [33] introduces a configuration for enabling the BL working of a wound rotor vernier motor using an additional 1-phase AW. In the proposed configuration, the stator comprises two sets of windings: 4-pole, main 3-Φ winding, and a 1-phase 2-pole auxiliary winding. The rotor, in turn, includes 44-pole RFW and 2-pole REW. The stator main winding generates FC-SMMF, while the auxiliary winding produces a SH-SMMF that induces current in the REW. This excitation winding is connected to a revolving rectifier. The RFW is supplied with DC, which is converted from the induced AC by the rectifier. Torque in rotor is produced by the electromagnetic interaction between the RFW and the main SW fields.

A BL excitation scheme for a WFSM is discussed in [34] based on the generation of an additional 2-pole MMF component using a series-connected auxiliary 3-Φ SW. Unlike conventional methods that employ inverter-based harmonic current injections, this approach utilizes a stator auxiliary winding connected in series with the main AW. The fundamental air-gap flux interacts with the rotor flux, while the auxiliary winding produces a rotating flux that induces voltage in RHW. The generated voltage is changed to DC with the help of a rectifier to inject DC excitation for RFW, enabling BL rotor excitation without a slip-ring assembly. The utilization of an additional stator-side winding and the presence of significant torque ripple are the major drawbacks of such topologies.

A BL synchronous machine topology based on the utilization of SH-SMMF is proposed in [35]. The machine employs a two-layer SW with two balanced 3-Φ windings and achieves brushless excitation using an auxiliary rotor winding induced by a one-fourth SH-SMMF. However, the proposed topology exhibited higher torque ripples of 34%, which is a major issue in this machine.

A dual-inverter configuration for the BLWFVM was proposed in [36] to enable BL operation. In this topology, two SWs (ABC and A2) are supplied by two inverters, which simultaneously generate the FC-SMMF and the SH-SMMF. The A2 winding (additional winding) is designed with the equal number of pole pairs as the REW, while the ABC winding has a different pole-pair number. The SH-SMMF induces an EMF in the REW, which is rectified and supplied to the RFW. However, the proposed motor involves two inverters and two SWs, which raises the overall cost, complexity, and size of the machine.

A hybrid BLWFSM (HBLWFSM) with an outer rotor topology is proposed, capable of operating both as a PMSM and as HBLWFSM [37]. A centrifugal switch is incorporated to enable switching between HBLWRSM and PMSM operation. Employing a concentrated winding, the machine comprises 48 poles, 36 stator slots, an outer rotor, and an inner stator. This machine is designed for dual-speed operation, e.g., in washing machines, running at 46 rpm (low speed) and 1370 rpm (high speed). When running at high speed, the PMSM mode is engaged to improve efficiency and reduce torque ripple. However, for the HBLWRSM, the torque ripple in dry mode is 98.5%, indicating a very high level of torque fluctuation.

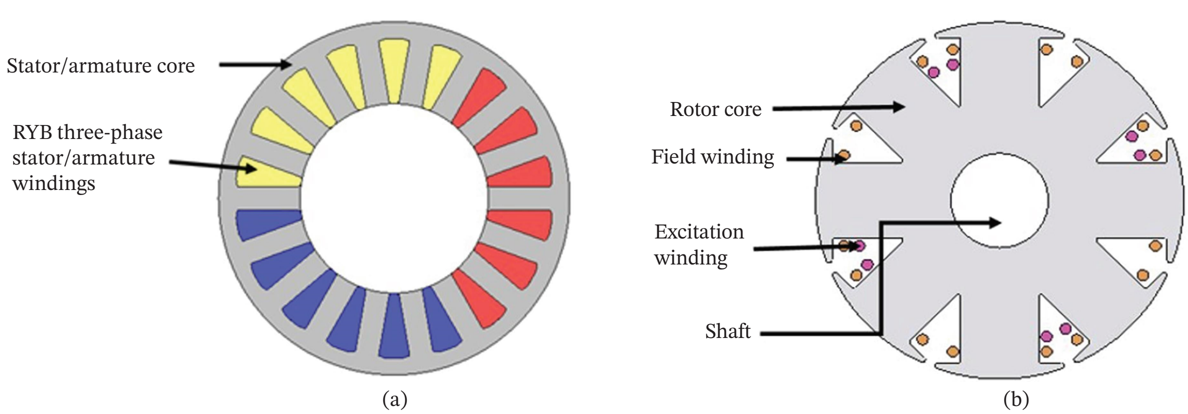

FIGURE 4 | (a) Stator of the proposed BLWFSM. (b) Rotor of the proposed BLWFSM.

TABLE 2 | Specifications of proposed BLWFSM.

Parameter	Units	Proposed BLWFSM
Power	W	746
Speed	Rev/min	900
3-Φ supply frequency	Hz	60
Stator outer/inner diameter	mm	177/95
Air gap	mm	0.5
Shaft diameter	mm	25
Stack length	mm	80
AW poles	—	8
No. of RFW poles	—	8
No. of slots available on stator for AW	—	18
Per-phase AW turns	—	240
RFW turns.	—	224
Turns of REW.	—	32
Material used for winding		Copper
Material used for core	—	50H1300

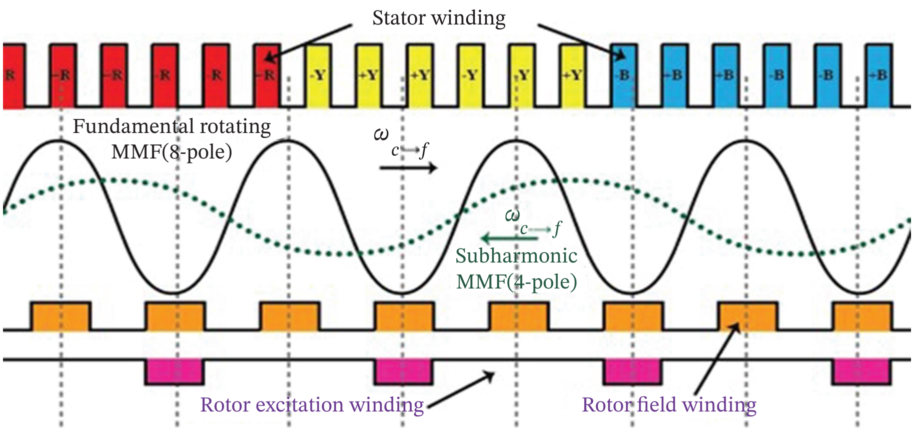

FIGURE 5 | Proposed machine stator and rotor winding arrangements.

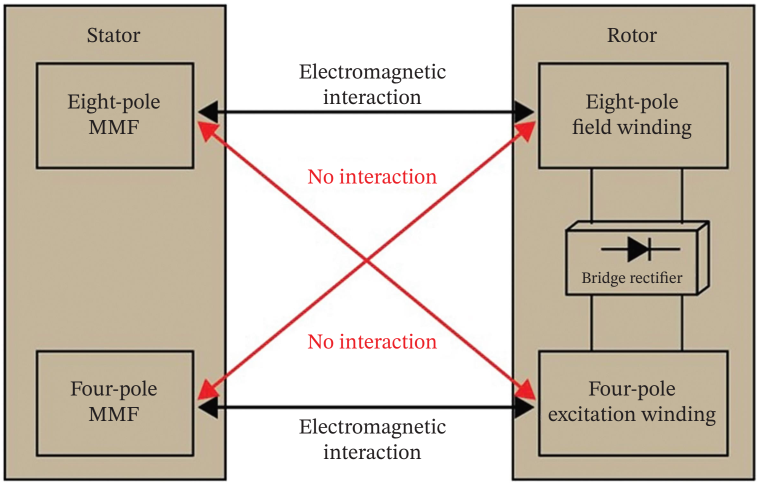

FIGURE 6 | Proposed 18-slot, 8-pole machine operating principle.

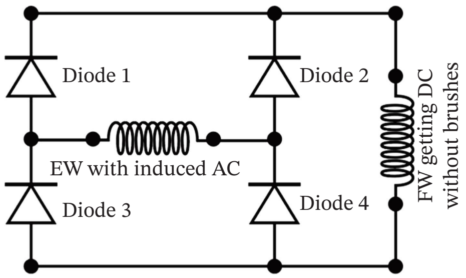

FIGURE 7 | Schematic configuration of REW, rectifier, and RFW.

A subharmonic field excitation technique based on a subharmonic MMF with one-fourth the magnitude of the fundamental MMF was proposed for the BL operation of WFSMs [38]. The topology employs a single inverter and a three-layer AW to generate the SH-MMF, which induces harmonic currents in the RHW. These currents are rectified to provide DC excitation to the RFW. An 8-pole, 48-slot motor was validated using FEA. However, the proposed motor exhibits a high torque ripple of approximately 32%.

From the above discussion and relevant literature, it is clear that many BL topologies employ either dual inverters or specially designed AW configurations to produce a harmonic MMF component required for BL operation. In either case, whether employing two inverters or implementing special SW configurations, the overall cost and size of the system increase. A highly efficient BLWFSM with a single-inverter, 1-layer AW configuration is presented in this paper. The 1-layer AW of the proposed machine generates both FC-SMMF and SH-SMMF within the air gap. The REW, bridge rectifier, and RFW are in series. The subharmonic field, rotating at twice the synchronous speed, induces a harmonic current in REW, which is rectified to excite RFW and thereby enable BL operation of the WFSM.

Existing literature indicates that conventional BL machine topologies often necessitate dual-inverter systems or complex SW configurations to induce the SH-SMMF required for BL operation. In either case, system dimensions and manufacturing costs are increased. This paper presents a novel high-efficiency BLWFSM that overcomes the cost and size constraints of traditional dual-inverter designs. The primary contributions of this design include the following:

- **Architectural Simplification:** A single-inverter, 1-layer AW that significantly reduces hardware overhead and system volume.
- **Harmonic Utilization:** The 1-layer AW of the proposed machine generates both FC-SMMF and SH-SMMF within the air gap to enable integrated self-excitation.
- **Integrated Rotor Design:** The REW and RFW on the rotor are series connected through a diode rectifier. The subharmonic field, rotating at twice the synchronous speed, induces a harmonic current in REW, which is rectified to excite RFW and thereby enable BL operation of the WFSM.

A comparative summary of the proposed BLWFSM and a conventional brushless generator with an embedded exciter is presented in Table 1. In a conventional brushless generator, excitation is achieved by employing an auxiliary AC exciter mounted on the same shaft, along with a rotating rectifier, and, in some cases, a pilot exciter is also present on the shaft, as shown in Figure 1. Although this arrangement eliminates brushes and slip rings, it increases system size, cost, weight, and structural complexity. In contrast, the proposed BLWFSM integrates the excitation mechanism within the main machine by utilizing an inherent SH-SMMF to induce voltage in the rotor excitation winding. This eliminates the need for a separate exciter and enables operation with a single three-phase inverter, resulting in a more compact and simplified structure.

The paper is structured in the following way. Section 2 introduces the proposed BL topology, machine configuration, and operating principle. Section 3 evaluates the machine's performance employing two-dimensional (2D) FEA to evaluate and compare it with the CWFSM and existing BLWFSM. Section 4 presents the conclusions.

2 | Proposed BLWFSM Topology, BLWFSM Configuration, and BLWFSM Operating Principle

2.1 | Proposed BLWFSM Topology

The proposed BLWFSM topology is based on an 8-pole, 18-slot machine and is validated using a 3-Φ AW with a 1-layer configuration. The rotor consists of 4 poles of the REW and 8 poles of

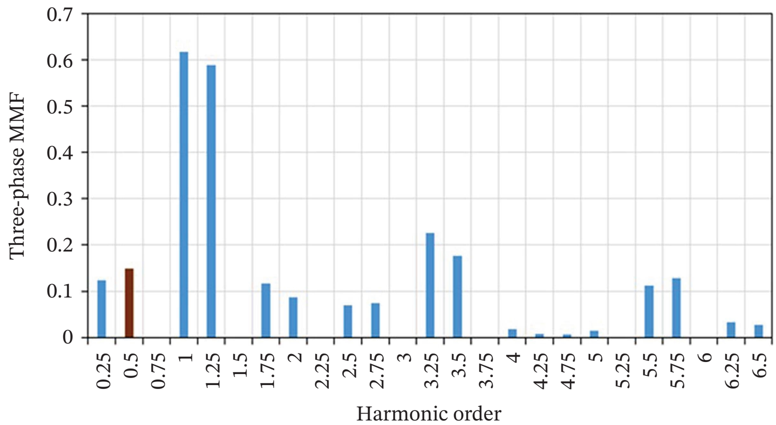

FIGURE 8 | Dominant harmonic components with MMF magnitude in proposed 18-slot/8-pole machine.

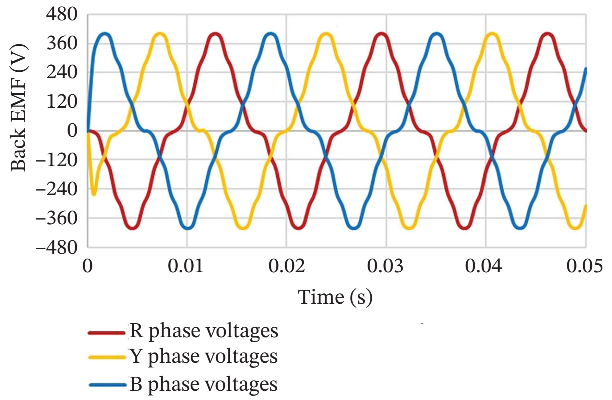

FIGURE 9 | Proposed 18-slot/8-pole machine: back EMF.

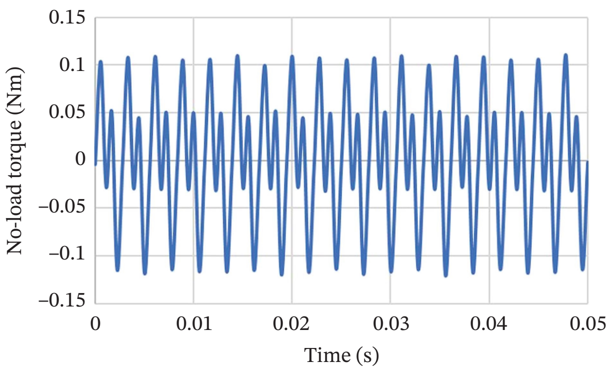

FIGURE 10 | Proposed 18-slot/8-pole machine: no-load torque.

the RFW. A balanced sinusoidal 3-Φ current of 60 Hz supplies the three-phase AW, producing a FC of 60-Hz MMF and SH-SMMF at various frequencies across the air gap of the machine. The 30-Hz subharmonic induces a voltage in the 4-pole REW, which is converted into DC through rectification, thereby exciting the 8-pole RFW without requiring brushes or slip rings. The stator's main magnetic field, generated by the FC-SMMF, rotates at synchronous speed. Torque is produced in the proposed BLWFSM by the coupling of the stator and rotor main magnetic fields. Figure 3 demonstrates the operation of the proposed topology under BL conditions.

2.2 | BLWFSM Configuration

An 8-pole, 18-slot BLWFSM with 3-Φ, 1-layer concentrated AW is designed to validate the proposed BL scheme. Figure 4a,b depict the complete machine layout, showing the stator and rotor winding configurations, respectively. The AW is excited using a balanced 3-Φ current provided by a single 3-Φ current source inverter. The design specifications for the proposed BLWFSM are listed in Table 2. The selection of the 18-slot/8-pole configuration is primarily motivated by its capability to inherently produce the required SH-SMMF, which is essential for realizing the proposed BL excitation principle. The rotor comprises two distinct windings: REW and RFW. In the proposed topology, the REW is designed to have a pole pitch twice that of the RFW. Consequently, the REW has four poles and is intended to interact with the 0.5-Hz SH-SMMF. Voltages induced in REW are rectified to feed DC into the RFW, generating the main rotor magnetic field. The 8-pole RFW is employed to synchronize the rotor field with the 8-pole stator field. The rotor and SWs, along with their

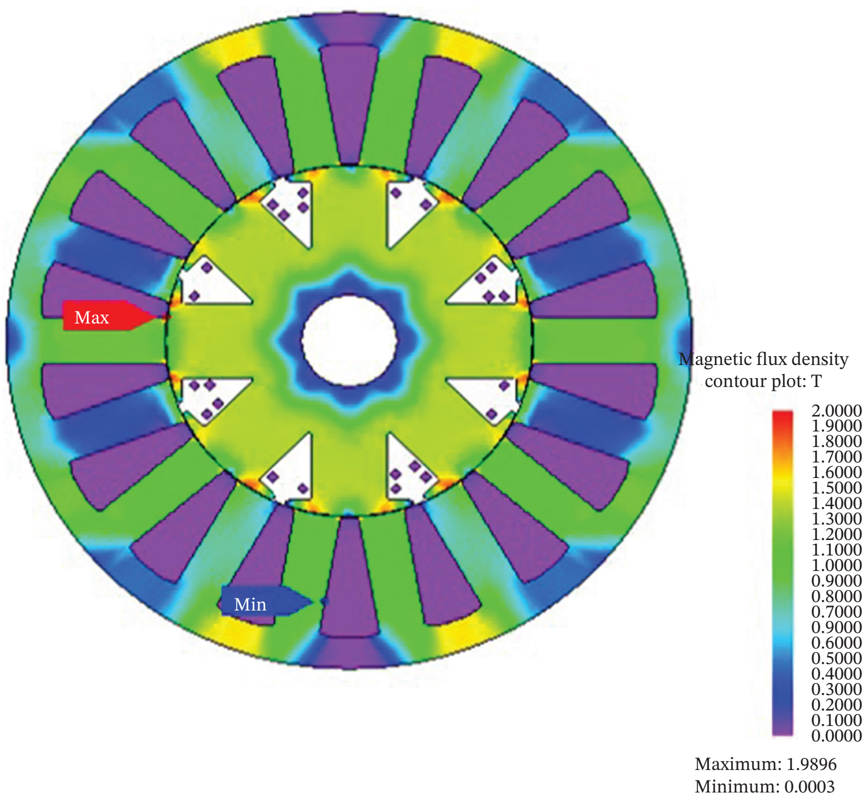

FIGURE 11 | Flux density plot of the proposed machine in no-load condition.

TABLE 3 | Proposed BLWFSM results under no load.

Parameters	Units	Proposed BLWFSM
Back EMF	Vrms	239.04
Peak cogging torque (absolute value)	Nm	0.11

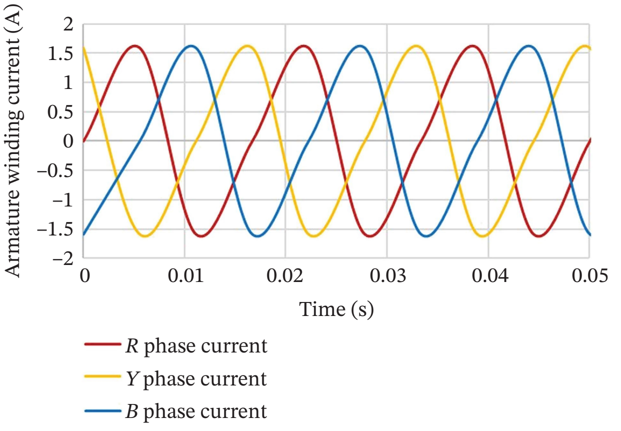

FIGURE 12 | Proposed machine input current fed to 3-Φ AW.

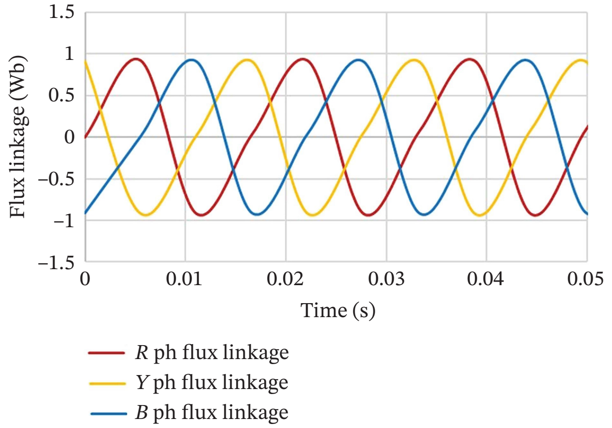

FIGURE 13 | Flux linkages with AW of proposed machine.

structures, are illustrated in Figure 5. The 50H1300 is a silicon steel core material used in the core of the proposed machine to improve efficiency and reduce energy loss.

2.3 | Operating Principle

The proposed design utilizes only a single inverter, unlike existing topologies that require two inverters. Furthermore, no additional windings are needed on the armature or stator side. In the proposed design, BL operation is achieved by the SH-SMMF generated when the 3-Φ AW is energized by a single 3-Φ inverter. The SH-SMMF, of 0.5 order and 30-Hz frequency, produces a rotating magnetic field that induces an AC voltage in the REW. This AC output is changed to DC using a rectifier, and the resulting DC is injected into the RFW without the use of brushes or slip rings. After receiving DC from the rectifier, the RFW produces the main rotor field of the motor. The working principle is illustrated in the block diagram as shown in Figure 6. The 3-Φ currents supplied to the AW for the proposed machine can be written as follows:

$$
\begin{aligned}
i_R(t) &= I_1 \sin\omega t, \\
i_Y(t) &= I_1 \sin\left(\omega t - \frac{2\pi}{3}\right), \\
i_B(t) &= I_1 \sin\left(\omega t + \frac{2\pi}{3}\right),
\end{aligned} \tag{1}
$$

where t, ω, and I_1 represent time, angular frequency, and the peak value of current supplied to the AW, respectively.

The speed of the FC-SMMF is 900 rpm, while the speed of the SH-SMMF is 1800 rpm, which is twice that of the FC-SMMF. Due to its higher speed, the SH-SMMF generates a voltage in REW in accordance with Faraday's law of electromagnetic induction. In this research, the number of poles of the SH-SMMF and the REW is equal; both have 4 poles, as specified in Table 2. Similarly, the pole count of the RFW must correspond to that of the FC-SMMF; both have 8 poles to ensure proper machine operation. Figure 7 presents the rotor schematic diagram, clearly showing the REW, rectifier, and RFW.

All harmonics present in the suggested machine are shown in Figure 8. The FC-SMMF at 60 Hz (1st harmonic order) and the SH-SMMF at 30 Hz (0.5 harmonic order) are used to obtain BL operation among all harmonics. The 0.5-order harmonic plays a key role in inducing voltage in the REW. The AC produced is ultimately rectified to DC by a rotor-mounted rectifier, and the resulting DC is supplied to the RFW without brushes. Consequently, the proposed machine operates under BL conditions. The harmonic spectrum of the air-gap MMF shows that the FC has a normalized magnitude of approximately 0.616, whereas the subharmonic component responsible for field excitation has a magnitude of approximately 0.15. So, the excitation MMF is approximately 19.35% of the fundamental MMF.

3 | 2D Finite Element Analysis of Proposed 18-Slot, 8-Pole Machine

3.1 | Proposed BLWFSM No-Load Analysis

To investigate no-load performance of the proposed 18-slot/8-pole machine, a no-load analysis was conducted using JMAG-Designer Version 18.1. A 1 A DC was injected into the RFW to establish the rotor magnetic field. The rotor speed was maintained at 900 rpm, as specified in Table 2. Under these conditions, the machine generates a back EMF of 239.04 Vrms, as illustrated in Figure 9. In addition, the machine exhibits a peak cogging torque of 0.11 Nm, as presented in Figure 10. The magnetic flux density distribution under no-load conditions is presented in Figure 11, indicating that the machine operates below the magnetic saturation limit, with a maximum flux density of 2 T. Table 3 presents the results of the proposed BLWFSM under no-load conditions.

3.2 | Proposed 18-Slot, 8-Pole BLWFSM Load Analysis

To verify the proposed BLWFSM topology, a 2D FEA of the 8-pole, 18-slot machine was carried out using JMAG-Designer.

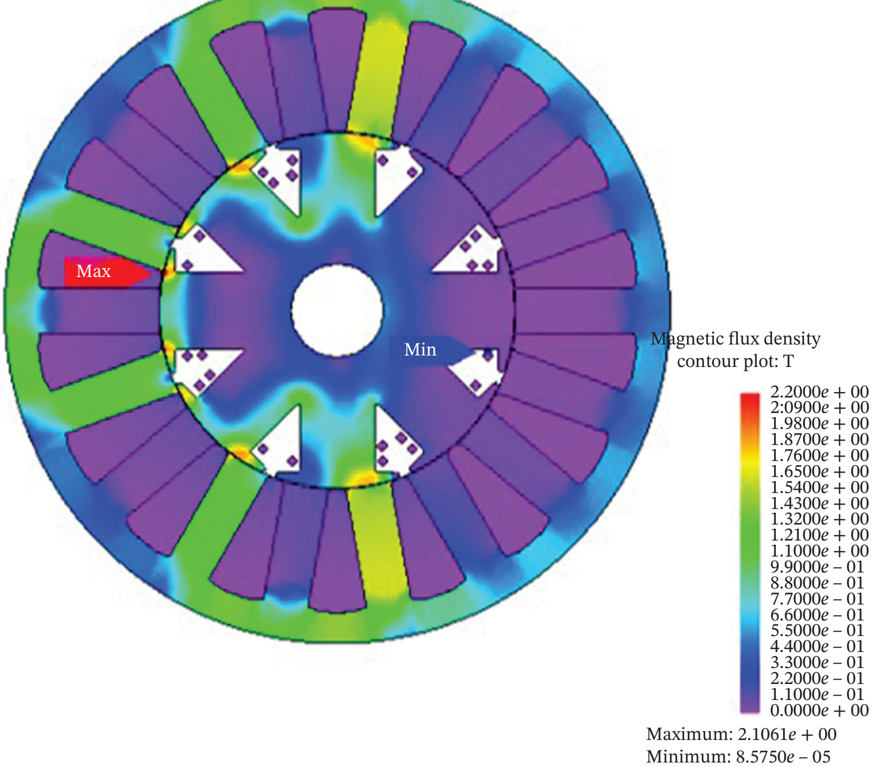

FIGURE 14 | Flux density plot of proposed machine in loaded condition.

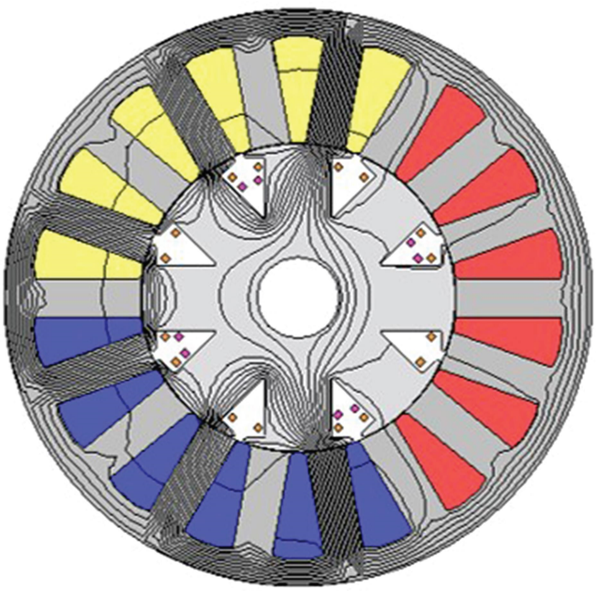

FIGURE 15 | Flux lines of proposed machine in loaded condition.

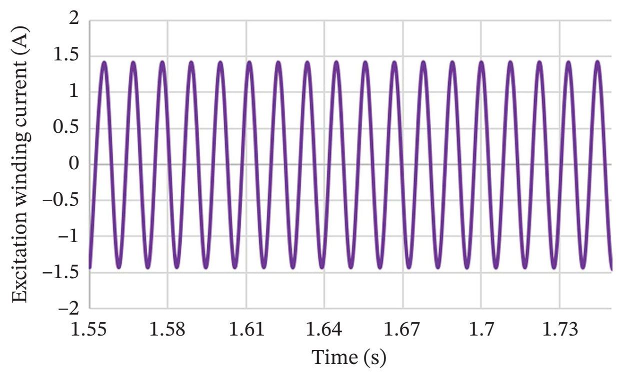

FIGURE 16 | AC in REW of proposed machine in loaded condition.

1.3 A_{rms} per-phase current was injected into the AW of the proposed machine. The 3-Φ currents injected to the AW are shown in Figure 12. The rotor rotates at a speed of 900 rpm, and the simulation was carried out for 3 s. Two main MMF components are present in the stator MMF: a 30-Hz SH-SMMF and a 60-Hz FC-SMMF. In the machine, the 60-Hz FC-SMMF generates the main stator magnetic field, while the 30-Hz SH-SMMF helps generate AC in the REW. Employing a rectifier placed between the REW and the RFW, the AC induced in the REW is converted into DC. Since the rectifier assembly is mounted on the rotor, the rectified DC output is directly supplied to the RFW without the use of brushes or slip rings. The flux linkage of the 3-Φ AW exhibits a sinusoidally varying magnetic field, as shown in Figure 13 for the proposed machine.

Figure 14 shows the magnetic flux density plots of the proposed 18-slot/8-pole machine, indicating that during loaded operation, the maximum flux density reaches approximately 2.106 T. This confirms that the machine operates within the permissible saturation limit, and no part of the machine experiences excessive magnetic saturation under load conditions. The flux line distribution of the proposed machine is illustrated in Figure 15. These flux lines complete the magnetic path from the stator through the air gap to the rotor, then return through the air gap to the stator, forming a closed magnetic path. The SH-SMMF is responsible for inducing AC in the REW according to Faraday's law of electromagnetic induction. The produced AC in the REW is also shown in Figure 16. Using a rectifier, this AC is converted into DC and supplied as the input to the RFW. The DC current in the RFW is shown in Figure 17. From Figures 16 and 17, it can be seen that the RMS value of the induced AC current in the REW is 1.43 A_{rms}, while the average DC supplied to the RFW is 1.43 A. Therefore, the proposed machine successfully provides DC excitation to the RFW without requiring brushes or slip rings, enabling fully BL operation.

The electromagnetic torque in the proposed machine is developed by the interaction between the main stator field, generated by the FC-SMMF, and the rotor field, established through the SH-SMMF. The developed output torque is shown in Figure 18. The average torque produced by the suggested machine is 8.975 N·m, as illustrated in Figure 18. To evaluate the torque ripple present in the output torque of the proposed machine, a zoomed view of the torque waveform is provided in Figure 19. The torque ripple is determined from the minimum, average, and maximum torque values. The corresponding values are 8.995 N·m (maximum torque), 8.95 N·m (minimum torque), and 8.975 N·m (average torque), respectively. Using (2), the torque ripple of the proposed machine is calculated to be 0.501%, indicating excellent performance and confirming the effectiveness of the proposed machine design.

The percentage torque ripple is calculated using the following equation:

$$\%\text{Torque ripple} = \frac{T_{max} - T_{min}}{T_{average}} \times 100, \tag{2}$$

where $T_{averageg}$, T_{max}, and T_{min} indicate the magnitudes of average, maximum, and minimum torques, respectively.

$$\begin{aligned} \%\text{Torque ripple} &= \frac{8.995 - 8.95}{8.975} \times 100, \\ \%\text{Torque ripple} &= 0.501. \end{aligned} \tag{3}$$

To calculate the percentage η of the proposed configuration, the following equations are used:

$$\%\eta = \frac{\text{Output power}}{\text{Input power}} \times 100, \tag{4}$$

$$\%\eta = \frac{P_{out}}{P_{out} + P_{loss}} \times 100, \tag{5}$$

where

$$P_{out} = \left(\frac{2\pi}{60}\right) NT, \tag{6}$$

$$P_{loss} = P_{cu\,loss} + P_{core\,loss}, \tag{7}$$

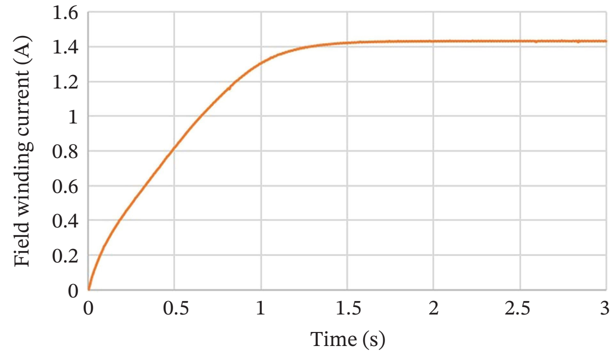

FIGURE 17 | DC in RFW of proposed 18-slot, 8-pole BL machine in loaded condition.

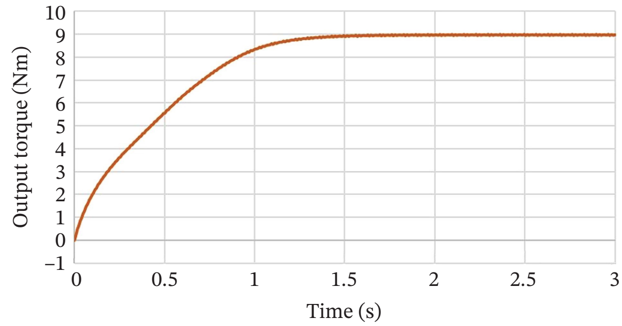

FIGURE 18 | Output torque of proposed 18-slot, 8-pole BL machine.

$$P_{cu\,loss} = P_{stat,cu} + P_{rfw,cu} + P_{rew,cu}, \tag{8}$$

where P_{out} and P_{loss} correspond to output power and the total power loss, respectively. The symbol N denotes the motor speed, while T indicates the average induced torque in the rotor of the proposed machine. Two types of losses occur in the proposed machine: core losses and copper losses. The total copper loss is the sum of three components: the SW copper loss ($P_{stat,cu}$), the RFW copper loss ($P_{rfw,cu}$), and the REW copper loss ($P_{rew,cu}$).

By substituting the values into Equations (4)–(8), the % efficiency ($\%\eta$) of the proposed machine can be calculated.

$$\begin{aligned} \%\eta &= \left[\frac{\{((2\pi)/60) \times 900 \times 8.975\}}{\{((2\pi)/60) \times 900 \times 8.975\} + \{63.88 + 12.168 + 4.58 + 2.045\}}\right] \times 100, \\ \%\eta &= \left[\frac{\{845.8738\}}{\{845.8738\} + \{63.88 + 12.168 + 4.58 + 2.045\}}\right] \times 100, \\ \%\eta &= \left[\frac{845.8738}{928.5468}\right] \times 100 = = 91.096\%. \end{aligned} \tag{9}$$

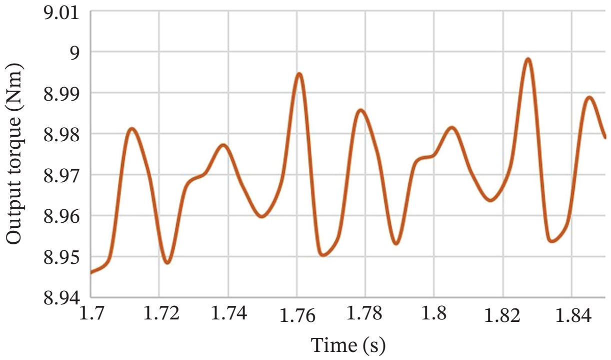

FIGURE 19 | Zoomed output torque of proposed 18-slot, 8-pole BL machine.

TABLE 4 | Detailed simulation results showing output torque, power, loss components, input power, and efficiency at different load conditions.

Sr. no.	Input current (A RMS)	Loading (%)	Output torque (Nm)	Output power (W)	Core loss (W)	Stator copper loss (W)	Field winding copper loss (W)	Excitation winding copper loss (W)	Input power (W)	Efficiency (%)
1	1.30	100 (rated load)	8.975	845.8738	63.88	12.168	4.58	2.049	928.5508	91.096
2	1.25	91.7	8.232	775.848	60.934	11.25	3.862	1.316	853.21	90.93
3	1.20	80.475	7.223	680.75	57.37	10.368	2.941	1.151	752.58	90.45
4	1.15	66.74	5.99	564.544	51.56	9.522	2	0.945	628.571	89.81
5	1.10	49.86	4.4755	421.81	44.30	8.712	1.0689	0.477	476.3679	88.547
6	1.05	39.98	3.589	338.255	40.166	7.938	0.671	0.3	387.33	87.33
7	0.975	30.1	2.7	254.47	35.84	6.844	0.3857	0.17	297.71	85.48
8	0.65	12.4	1.112	104.80	22.33	3.042	0.132	0.06	130.36	80.41
9	0.325	2.91	0.261	24.6	7.08	0.761	0.033	0.0146	32.49	75.71

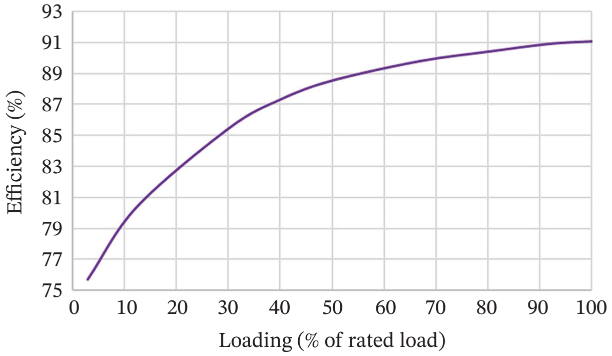

FIGURE 20 | Variation of efficiency from no-load to rated-load condition.

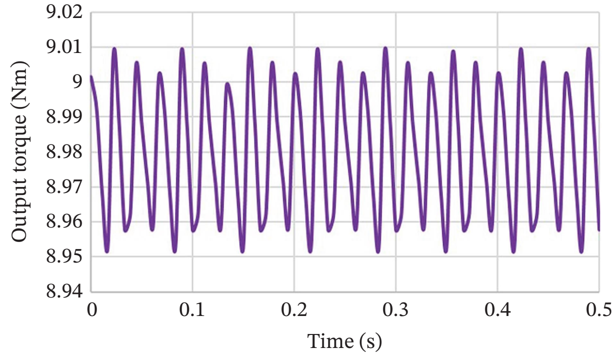

FIGURE 21 | Output torque of CWFSM.

To address the variation of machine performance under different loading conditions, simulations were carried out at multiple RMS input current levels. The rated operating condition corresponds to 1.3 A RMS, while lower current values (1.25 A, 1.20 A, etc.) represent progressively lighter load conditions. The corresponding performance metrics, including output power, input power, and efficiency, are summarized in Table 4.

The inverter rating is determined from the stator input power of 928 W obtained from simulation results. Considering unity power factor operation and a 50% safety margin for transient and design robustness, the inverter is selected with a rating of approximately 1.4 kVA. Alternatively, the proposed machine can also be operated directly from a conventional three-phase AC supply without requiring a dedicated inverter, provided that the required stator current is maintained.

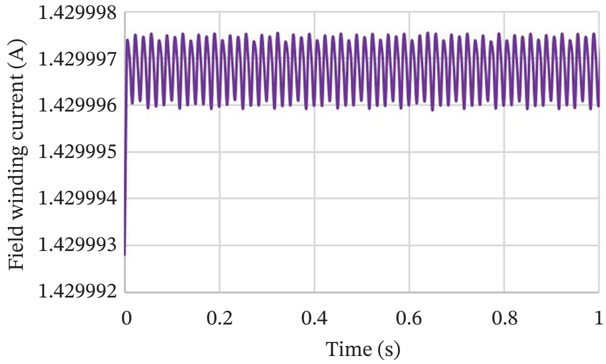

FIGURE 22 | RFW current of CWFSM.

TABLE 5 | Performance comparison of CWFSM and proposed BLWFSM.

Parameter	Units	CWFSM	Proposed BLWFSM
Per-phase AW current	Arms	1.3	1.3
Induced torque	Nm	8.9797	8.975
Torque ripples	%	0.445	0.501
Current of RFW	A	1.43	1.43
Current of REW	Arms	NA	1.43
Core loss	W	67.3	63.88
Cu loss of AW	W	12.168	12.168
Cu loss of RFW	W	4.58	4.58
Cu loss of REW	W	NA	2.045
Efficiency	%	91	91.096

TABLE 6 | Comparative performance assessment of the proposed and existing BLWFSMs [39].

Parameters	Units	Existing BLWFSM [39]	Proposed BLWFSM	% improvement in proposed BLWFSM
Output power	W	777	845.8738	8.68
Average torque	Nm	8.24	8.975	8.92
Torque ripples	%	18.41	0.501	−97.28
AW current (per phase)	A_{rms}	4.5	1.3	−71.11

Furthermore, to provide a clearer visualization of the efficiency trend with respect to load variation, the efficiency values are plotted against the percentage of loading. Figure 20 illustrates the variation of efficiency as the operating condition moves from very light-load (nearly no load) to rated-load conditions, demonstrating the performance behavior of the machine over the considered operating range.

3.3 | Comparative Analysis Between the CWFSM and the Proposed BLWFSM Configuration

The output torque and other performance parameters of the proposed BL motor were compared with those of the CWFSM. In a CWFSM, the RFW is energized with DC power supplied from an external source. This DC excitation is delivered to the RFW through carbon brushes and slip rings; therefore, the CWFSM is also referred to as a brushed WFSM. To ensure a fair comparison between the two machines—the brushed WFSM (CWFSM) and the proposed BLWFSM—certain parameters were kept constant for both machines. Both machines operate at the same speed of 900 rpm. The air-gap length, rotor and stator inner and outer diameters, and the number of turns for the REW, RFW, and AW are identical for both machines. In addition, the number of poles for the REW and RFW is the same in both cases. The winding and core materials are also identical for the CWFSM and the proposed BLWFSM. The only difference between the two machines lies in the method of supplying DC power to the RFW. In the CWFSM, the DC excitation is supplied to the RFW from an external DC source through brushes. In contrast, in the proposed BLWFSM, the DC supply is obtained from the rectifier output. Figure 21 shows the output torque of the CWFSM, while Figure 22 depicts the DC current supplied to RFW from an external source via brushes and slip rings. Table 5 provides a comprehensive comparison of the performance characteristics between the CWFSM and the proposed BLWFSM.

3.4 | Comparative Analysis of the Existing BLWFSM [39] and the Proposed BLWFSM

To enable a fair comparison between the existing design [39]and the proposed BLWFSM, both machines are evaluated under identical design constraints. 50H1300 core material is used in both designs. Both machines share identical outer and inner stator diameters, a 0.5 mm air-gap length, and a 25 mm shaft diameter. The operating speed of each machine is 900 rev/min., while the per-phase AW turns, RFW turns, and REW are maintained at the same values. Additionally, both machines are designed with a stack length of 80 mm.

Table 6 presents the results of the comparative assessment of the proposed BLWFSM and the existing BLWFSM [39]. The proposed BLWFSM achieves an 8.92% higher average torque and 8.86% higher output power while operating with 71.11% lower AW current compared to the existing configuration [39]. Moreover, the torque ripple of the proposed machine is reduced by approximately 97.28% relative to the existing design [39]. The improvements in average torque and output power, together with the significant reduction in torque ripple while utilizing lower input current, demonstrate the superior performance of the proposed BLWFSM over the existing design [39].

4 | Conclusion

This article presents a BLWFSM topology that exploits the 0.5-order (30 Hz) SH-SMMF present in the air gap to enable BL field excitation. The proposed machine's stator has 18 slots for the AW, which is supplied with power either through a conventional 3-Φ AC source or from a single 3-Φ inverter. The proposed machine employs a rotor configuration with an 8-pole RFW and a 4-pole REW. The inherent SH-SMMF of 0.5 order (30 Hz) is exploited to produce an alternating current in the REW. A rectifier is incorporated between the REW and the RFW to convert the AC induced in the RHW into DC, which is subsequently fed to the rotor RFW without using brushes or slip rings. Thus, the proposed eight-pole, 18-slot machine operates in brushless manner. The torque in the proposed WFSM is produced by the electromagnetic interaction between the stator main magnetic field, generated by the 60-Hz FC-SMMF, and the magnetic field produced by the RFW.

The performance of the proposed BLWFSM is evaluated using 2D FEA in JMAG. The results are compared with a CWFSM, where the RFW is powered by an external DC source via carbon brushes and slip rings. The proposed machine exhibits performance that is in close agreement with the CWFSM, highlighting the effectiveness of the proposed BL topology. However, the proposed machine operates in a brushless manner. Additionally, the torque ripples in the proposed machine are less than 1%, which is another strong indication of the effectiveness of the topology presented in this research. The proposed BLWFSM, when compared to the existing BLWFSM, demonstrates superior overall performance by achieving higher average torque and output power with significantly lower AW current and substantially reduced torque ripple. The proposed topology can serve as a replacement for PMSMs or CWFSMs, particularly in applications, such as air blowers and aircraft power generation, where low volume and weight are critical. Furthermore, with appropriate design modifications, the topology is suitable for use in electric vehicles, allowing efficient operation over a wide speed range.

Nomenclature

3HC-SMMF	Third harmonic component of stator MMF
AW	Armature winding
BL	Brushless
BLWFSM	Brushless wound-field synchronous machine
CWFSM	Conventional wound-field synchronous machine
EW	Excitation winding
FC	Fundamental component
FC-SMMF	Fundamental component of stator MMF
MMF	Magnetomotive force
PM	Permanent magnet
PMSM	Permanent magnet synchronous machine
REW	Rotor excitation winding
RFW	Rotor field winding
RHW	Rotor harmonic winding
SH-SMMF	Subharmonic component of stator MMF
SW	Stator winding
WFSM	Wound-field synchronous machine

Author Contributions

Muhammad Ahsan ul Haq: conceptualization, software simulation, validation, writing, data curation, review and editing, visualization, and resources.

Haroon Farooq: validation, writing, data curation, review and editing, visualization, and supervision.

Muhammad Akmal: supervision and writing–review and editing.

Acknowledgments

The authors acknowledge their respective parent universities for granting access to research facilities used in this study.

Funding

The authors have nothing to report.

Disclosure

All authors reviewed the final draft and agreed to its contents.

Conflicts of Interest

The authors declare no conflicts of interest.

Data Availability Statement

All the necessary data have been included in the manuscript.

References

1. T. He, Z. Zhu, F. Eastham, et al., "Permanent Magnet Machines for High-Speed Applications," *World Electric Vehicle Journal* 13, no. 1 (2022): 18, https://doi.org/10.3390/wevj13010018.

2. M. Bahrami-Fard, T. Chen, E. A. Winchell, and B. Fahimi, "Integrated Induction Motor Drive for Variable Speed Industrial Applications," *IEEE Transactions on Power Electronics* 40, no. 5 (2025): 7176–7188, https://doi.org/10.1109/tpel.2025.3532880.

3. K. B. Tawfiq, "Performance Enhancement in Rewound Industrial Retrofit Solutions for Five-and Six-Phase Permanent Magnet Assisted Synchronous Reluctance Machines," *IEEE Transactions on Industry Applications* 62 (2025).

4. O. A. Badewa, "Electromagnetic Design Characterization of Synchronous Machines With Flux Switching Effect Employing Reluctance Rotors and Stators With PMs and AC Concentrated Coils," *IEEE Transactions on Industry Applications* 61 (2025).

5. M. Waldner and I. Erlich, "Variable Speed Wind Turbines Based on Electromechanical Differential Systems," *IEEE Transactions on Energy Conversion* 29, no. 1 (2013): 101–109, https://doi.org/10.1109/tec.2013.2287260.

6. W. Kellenberger, *IEE Proceedings C (Generation, Transmission and Distribution)* (IET), 137–141.

7. A. Fathelkhair, H. Abouobaida, Y. Mchaouar, Y. Abouelmahjoub, K. Oualifi, and J. M. Guerrero, "Sensorless Nonlinear Control of Permanent Magnet Synchronous Generator Based Wind Energy Conversion Systems," *Electrical Engineering* 107, no. 8 (2025): 9921–9948, https://doi.org/10.1007/s00202-025-03008-8.

8. S. M. Abbas, J. Ikram, Z. Ayub, T. Yazdan, and M. R. Siddiqi, "Brushless Operation of Axial-Flux Wound-Rotor Synchronous Machine Utilizing Third Harmonic," *Mathematics* 13, no. 24 (2025): 3936, https://doi.org/10.3390/math13243936.

9. S. Ahmed, M. R. Siddiqi, Q. Ali, T. Yazdan, A. Hussain, and J. Hur, "Brushless Wound Rotor Synchronous Machine Topology Using Concentrated Winding for Dual Speed Applications," *IEEE Access* 11 (2023): 119560–119567, https://doi.org/10.1109/access.2023.3327525.

10. M. Ayub, A. Hussain, G. J. Sirewal, and B.-I. Kwon, "Wye-Delta Winding Configuration for Brushless Operation of a Wound Field Synchronous Machine," *International Journal of Applied Electromagnetics and Mechanics* 64, no. 1–4 (2020): 1165–1172, https://doi.org/10.3233/jae-209433.

11. M. Ayub, G. Jawad, and B.-I. Kwon, "Consequent-Pole Hybrid Excitation Brushless Wound Field Synchronous Machine With Fractional Slot Concentrated Winding," *IEEE Transactions on Magnetics* 55, no. 7 (2019): 1–5, https://doi.org/10.1109/tmag.2018.2890509.

12. A. Roshanzamir, K. Y. Hwang, S. H. Lee, J. W. Kwon, M. Ayub, and B. I. Kwon, "Dual-Mode Brushless Wound Rotor Synchronous Machine for High Starting Torque," *IEEE Access* 10 (2022): 41657–41663, https://doi.org/10.1109/access.2022.3167886.

13. F. Arif, A. Arif, Q. Ali, et al., "A Novel Rotor Harmonic Winding Configuration for the Brushless Wound Rotor Synchronous Machine," *World Electric Vehicle Journal* 15, no. 6 (2024): 226, https://doi.org/10.3390/wevj15060226.

14. M. Humza, T. Yazdan, Q. Ali, and H.-W. Cho, "Brushless Operation of Wound-Rotor Synchronous Machine Based on Sub-Harmonic Excitation Technique Using Multi-Pole Stator Windings," *Mathematics* 11, no. 5 (2023): 1117, https://doi.org/10.3390/math11051117.

15. G. J. Sirewal, M. Ayub, S. Atiq, and B.-I. Kwon, "Analysis of a Brushless Wound Rotor Synchronous Machine Employing a Stator Harmonic Winding," *IEEE Access* 8 (2020): 151392–151402, https://doi.org/10.1109/access.2020.3017102.

16. A. Hussain, S. Atiq, and B.-I. Kwon, "Consequent-Pole Hybrid Brushless Wound-Rotor Synchronous Machine," *IEEE Transactions on Magnetics* 54, no. 11 (2018): 1–5, https://doi.org/10.1109/tmag.2018.2837690.

17. A. Hussain, Z. Baig, W. Toor, et al., "Wound Rotor Synchronous Motor as Promising Solution for Traction Applications," *Electronics* 11, no. 24 (2022): 4116, https://doi.org/10.3390/electronics11244116.

18. A. Fayyaz, F. Mehmood, C. M. Arbab Waheed, and Z. Ullah, "Novel Winding Design and Analysis of Brushless Wound Rotor Synchronous Machines," *IET Electric Power Applications* 19, no. 1 (2025): e70019, https://doi.org/10.1049/elp2.70019.

19. M. S. H. Rafin, Q. Ali, H. Hussein, and O. A. Mohammed, "Optimized Design of Sub-Harmonic Synchronous Machines," *IEEE Transactions on Magnetics* (2025).

20. Y. Xia, J. Xu, J. Hu, Y. Yu, Y. Chen, and J. Zhang, "Influence of Parameters on the Excitation Power of Third Harmonic Brushless Hybrid Excitation Generator," *Energies* 17, no. 23 (2024): 6021, https://doi.org/10.3390/en17236021.

21. F. Kutt, M. Michna, and G. Kostro, "Non-Salient Brushless Synchronous Generator Main Exciter Design for More Electric Aircraft," *Energies* 13, no. 11 (2020): 2696, https://doi.org/10.3390/en13112696.

22. B. Zaker, A. Khodadadi, and M. Karrari, "A New Approach to Parameter Identification of Generation Unit Equipped With Brushless Exciter Using Estimated Field Voltage," *International Journal of Electrical Power & Energy Systems* 141 (2022): 108122, https://doi.org/10.1016/j.ijepes.2022.108122.

23. Z. U. Din, J. Wang, J. Zhang, and X. Song, in *Proceedings of the 7th Asia Energy and Electrical Engineering Symposium (AEEES)* (Chengdu, China: IEEE, 2025), 360–364.

24. S. M. Gomaa, A. A. Mohamed, and M. M. Khater, in *Proceedings of the 26th International Middle East Power Systems Conference (MEPCON)* (Aswan, Egypt: IEEE, 2025), 1–6.

25. M. Ayub, S. S. H. Bukhari, G. Jawad, and B.-I. Kwon, "Brushless Wound Field Synchronous Machine With Third-Harmonic Field Excitation Using a Single Inverter," *Electrical Engineering* 101, no. 1 (2019): 165–173, https://doi.org/10.1007/s00202-019-00763-3.

26. S. S. H. Bukhari, H. Ahmad, F. Akhtar, and J. S. Ro, "Brushless Field-Excitation Method for Wound-Rotor Synchronous Machines," *International Transactions on Electrical Energy Systems* 31, no. 8 (2021): e12961, https://doi.org/10.1002/2050-7038.12961.

27. H. T. Ali, A. S. Abdel-Khalik, T. Al Saadi, and S. Ahmed, "Design and Electromagnetic Analysis of a Rare-Earth-Free Five-Phase 20-Slot/18-Pole Self-Excited Brushless Synchronous Machine," *Energies* (2026).

28. J. Chung and H. Hofmann, "Brushless Self-Excited Synchronous Field-Winding Machine With Five-and Higher-Phase Design Using Independently Controlled Spatial Harmonics," *IEEE Transactions on Energy Conversion* (2023).

29. Q. Ali, T. A. Lipo, and B.-I. Kwon, "Design and Analysis of a Novel Brushless Wound Rotor Synchronous Machine," *IEEE Transactions on Magnetics* 51 (2015): 1–4.

30. S. S. H. Bukhari, H. Ahmad, G. J. Sirewal, and J.-S. Ro, "Simplified Brushless Wound Field Synchronous Machine Topology Based on a Three-Phase Rectifier," *IEEE Access* 9 (2021): 8637–8648, https://doi.org/10.1109/access.2021.3049561.

31. S. S. H. Bukhari, G. J. Sirewal, F. A. Chachar, and J.-S. Ro, "Brushless Field Excitation Scheme for Wound Field Synchronous Machines," *Applied Sciences* 10, no. 17 (2020): 5866, https://doi.org/10.3390/app10175866.

32. H. M. Munir, Q. Ali, J. Rodriguez, and M. Abdelrahem, "Brushless Synchronous Machine With Dual-Frequency Inverter for High Torque and Low Ripple Operation," *IEEE Access* 13 (2025).

33. M. Humza, T. Yazdan, M. R. Siddiqi, and H.-W. Cho, "Brushless Wound Rotor Vernier Motor Using Single-Phase Additional Winding on Stator for Variable Speed Applications," *IEEE Access* 11 (2023): 86262–86270, https://doi.org/10.1109/access.2023.3304017.

34. G. J. Sirewal and S. S. H. Bukhari, "Cost-Effective Scheme for a Brushless Wound Rotor Synchronous Machine," *World Electric Vehicle Journal* 12, no. 4 (2021): 194, https://doi.org/10.3390/wevj12040194.

35. S. S. H. Rafin, Q. Ali, S. Khan, and T. A. Lipo, "A Novel Two-Layer Winding Topology for Sub-Harmonic Synchronous Machines," *Electrical*

Engineering 104, no. 5 (2022): 3027–3035, https://doi.org/10.1007/s00202-022-01531-6.

36. K. Kumar, "Performance Improvement of Brushless Wound Rotor Vernier Motor for Washing Machine Applications," *IEEE Access* 13 (2025).

37. S. Ahmed, Q. Ali, G. J. Sirewal, K. Kumar, and G. Choi, "Hybrid Brushless Wound-Rotor Synchronous Machine With Dual-Mode Operation for Washing Machine Applications," *Machines* 13, no. 5 (2025): 342, https://doi.org/10.3390/machines13050342.

38. S. S. H. Rafin, Q. Ali, and T. A. Lipo, "A Novel Sub-Harmonic Synchronous Machine Using Three-Layer Winding Topology," *World Electric Vehicle Journal* 13, no. 1 (2022): 16, https://doi.org/10.3390/wevj13010016.

39. M. Ayub, S. Atiq, Q. Ali, A. Hussain, and B.-I. Kwon, "Dual-Mode Wound Rotor Synchronous Machine for Variable Speed Applications," *IEEE Access* 8 (2020): 115812–115822, https://doi.org/10.1109/access.2020.2999609.